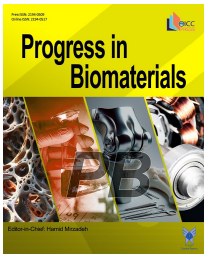

Volume 13, Issue 3, 132411 (1-13)

Progress in Biomaterials (PIBM)

https://doi.org/10.57647/pibm.2024.132411

Synthesis and Kinetic Study of Ion-Doped Zif-8 Nanocarriers for a Flutamide Delivery

Noushita Gilianinezhad[1], Hoda Pasdar[1], Mohammad Yousefi[2,*], Mandana Saber-Tehrani[1], Malak Hekmati[3]

[1]*Department of Chemistry, NT.C., Islamic Azad University, Tehran, Iran.*
[2]*Department of Chemistry, TeMS.C., Islamic Azad University, Tehran, Iran.*
[3]*Department of Pharmaceutical Chemistry, TeMS.C., Islamic Azad University, Tehran, Iran.*

[*]**Corresponding author:** myousefi50@iau.ac.ir

Original Research

Abstract:

Here, we describe characterization of new Zif-8 composites doped with magnetite (Fe_3O_4) and gold (Au) nanoparticles, labeled Zif-8-Fe and Zif-8-Au, to precisely tune their release kinetics, drug loading, and porosity. Geometry modification was observed in SEM images after ion doping, with the mean size ranging from 50-80 nm for Zif-8 and Zif-8-Au and about 500 nm for Zif-8-Fe. A clear XRD peak shift confirmed the successful incorporation of dopant ions. Brunauer-Emmett-Teller (BET) analysis revealed that while Au doping significantly reduced the material's surface area and pore volume, Fe doping remarkably enhanced these properties (556 vs 2676 m^2/g and 0.26 vs 1 cm^3/g, respectively). This directly impacted drug loading, with the Zif-8-Fe composite demonstrating the highest loading capacity (18.8 mg/g) and Zif-8-Au showing the lowest (7.2 mg/g). In vitro drug release studies further demonstrated distinct kinetic profiles. The release from all samples followed a Fickian diffusion mechanism, as indicated by the Korsmeyer-Peppas model ($n \approx 0.01 - 0.05$). The Zif-8-Fe composite exhibited a desirable sustained-release profile due to its enhanced and more tortuous pore network, while the Zif-8-Au composite showed low-quantity release. The findings demonstrated that ion doping provided a powerful strategy to engineer the structural properties and drug release kinetics of MOFs.

Keywords:

Nanoparticles; Drug delivery; Metal–organic framework (MOF); Cancer therapy

Cite this article: Gilianinezhad, N., Pasdar, H., Yousefi, M., Saber-Tehrani, M., Hekmati, M. Zamanlui Benisi, S., Hesami Tackallou, S., Mohammadi Shabestari, S., Nasrolah, M. H., Goodarzi, V. Synthesis and Kinetic Study of Ion-Doped Zif-8 Nanocarriers for a Flutamide Delivery. *Progress in Biomaterials* **13**(3), Article 11 (2024).

1. Introduction

The development of innovative drug delivery systems (DDS) that surpass traditional methods has garnered significant attention in recent years. Poor bioavailability, quick clearance, and lack of specificity are some of the drawbacks of conventional administration systems that might decrease therapeutic efficacy and increase adverse effects. In order to address these obstacles, researchers are creating novel drug delivery systems that are multipurpose in addition to being effective at delivering therapeutic drugs. Targeted distribution, controlled release, imaging capabilities, and even therapeutic monitoring are just a few of the characteristics that these sophisticated systems may incorporate, increasing their potential uses in contemporary medicine (Faheem and Abdelkader, 2020).

Nanomaterials have been identified as one of the most promising options for improved medication delivery among several approaches investigated (Teleanu et al., 2019). They are perfect for more effectively transporting medicinal substances because of their adjustable size, high surface area, and simplicity of surface modification (Panda et al., 2020). The very poor drug loading capacity of traditional nanoparticle-based drug delivery systems is one of the primary obstacles they confront, despite notable advancements in nanomedicine. Because of their small internal volume or few interaction sites, many nanoparticles, including liposomes, polymeric micelles, and inorganic carriers, can only contain a small number of therapeutic compounds (Bhardwaj et al., 2023). Because of this restriction, greater dosages of carriers are frequently needed to reach therapeutic medication levels, which might jeopardize patient safety by increasing toxicity and decreasing biocompatibility. Low loading efficiency can also result in inferior

treatment effects, poor stability during circulation, and early drug leakage (Panda et al., 2020; Bhardwaj et al., 2023). To optimize loading efficiency and controlled release, these disadvantages underscore the necessity of creating sophisticated nanocarriers with large surface area, adjustable porosity, and potent drug–carrier interactions.

Metal–organic frameworks (MOFs) are a class of porous crystalline materials composed of metal ions and organic linkers that have attracted growing attention due to their high loading capacity, structural flexibility, and biocompatibility (Freund et al., 2021). Several MOFs have been widely explored for drug delivery due to their high surface area, tunable pore sizes, and biocompatibility. For instance, Zif-8 (a zeolitic imidazolate framework) is commonly used because it offers pH-responsive release, making it ideal for targeting tumor environments (Wang et al., 2020). MIL-100(Fe) and MIL-101(Cr) are also popular choices, as their large pore volumes can encapsulate bulky drug molecules, such as doxorubicin and ibuprofen (Quintero-Álvarez et al., 2022). Similarly, UiO-66 (zirconium-based MOF) is valued for its exceptional stability and controlled drug release properties (Pourmadadi et al., 2023). In addition, bio-compatible frameworks such as Bio-MOF-1 have been investigated for the sustained release of therapeutic agents. Collectively, these MOFs highlight the versatility of framework design in tailoring drug delivery systems. Usually, one-pot or solvent-assisted linker exchange (SALE) techniques are used to create Zif-8 nanocarriers, which enable the addition of different ions or functional groups. As shown with 5-fluorouracil (5-FU), amine functionalization, which is accomplished by substituting 2-methylimidazole with 3-amino-1,2,4-triazole, improves drug encapsulation and alters release characteristics (Reshimi et al., 2023). Zif-8 nanocarriers also demonstrate pH-responsive drug release, showing accelerated release under acidic conditions because the framework degrades more rapidly. This behavior is particularly useful for targeting the acidic tumor microenvironment. Additionally, incorporating functional groups (such as amines) or doping ions into the structure can slow or fine-tune the release rate by enhancing host–guest interactions. Kinetic analyses further indicate that factors such as the metal-to-ligand ratio, the type of metal precursor used, and surface modifications (for example, coating with polyvinylpyrrolidone or LDH layers) play key roles in determining both drug-loading efficiency and release behavior (Gao et al., 2023; Wang et al., 2023).

Apart from improving drug loading capacity, the design and synthesis of multifunctional nanoparticles have gained considerable attention in recent years (Sanvicens and Marco, 2008). Such nanocarriers are not only capable of transporting therapeutic agents but can also be engineered to integrate additional functions, including targeted delivery, imaging, stimuli-responsive release, and synergistic therapeutic modalities (Bao et al., 2013). This multifunctionality enables precise drug accumulation at the diseased site, reduces off-target effects, and facilitates real-time monitoring of treatment efficacy (Sanvicens and Marco, 2008). Moreover, by combining diagnostic and therapeutic features within a single platform, multifunctional nanoparticles hold great promise for advancing personalized and more effective treatments in cancer and other complex diseases.

Flutamide is a non-steroidal anti-androgen with poor aqueous solubility ($\log P \approx 2.2 - 2.4$) and limited bioavailability, which significantly restricts its therapeutic performance in systemic administration. The drug has a pKa of approximately 11, meaning it remains largely unionized under physiological conditions, further contributing to its low solubility and slow dissolution rate. These physicochemical characteristics make Flutamide an excellent candidate for encapsulation within nanocarriers that can enhance its dispersion and controlled release (Lou et al., 2023; Tongeren et al., 2022).

One promising class of multifunctional nanocarriers is magnetic nanoparticles useful for magnetic targeting or hyperthermia applications (Dobson, 2006). The combination of high drug loading capacity with magnetic functionality can lead to a novel version of multifunctional nanoparticles for cancer therapy. The main aim of this study is to dope Au ions and Fe_3O_4 into Zif-8 to synthesize a new version of magnetic MOFs. These nanoparticles were then employed to load flutamide and evaluated from the viewpoint of drug release and kinetics. doping with Fe and Au enables fine-tuning of pore architecture, defect chemistry, surface energy, and binding site availability, all of which contribute to improved drug loading capacity and potentially more favorable release behavior compared to undoped Zif-8.

2. Materials and methods

2.1 Chemicals

All chemicals and reagents were of analytical grade and used as received. Zinc nitrate hexahydrate ($Zn(NO_3)_2 \cdot 6H_2O$) was sourced from Merck. 1 2-methylimidazole (MIM, $C_4H_6N_2$) with a purity of 99% was obtained from Sigma Aldrich. For the synthesis of Zif-8-Au, a gold salt (e.g., gold sodium chloride) was utilized, along with sodium borohydride ($NaBH_4$) from Spectrum Chemical Manufacturing.

2.2 Synthesis of nanoparticles (Zif-8, Au@Zif-8, Fe_3O_4@Zif-8)

Zif-8: First, 3 g of hexahydrate zinc nitrate were dissolved in 200 mL of methanol (solution 1). Then, 7 g of 2-methylimidazole (MIM) were dissolved in 100 cc of methanol (solution 2). Now, solution 1, which contains zinc ions, was added quickly and all at once to solution 2 and stirred for 2 hours. Then, it was centrifuged at 4000 rpm and washed with methanol. Then, the precipitate was dried in it. Molar ratio: MIM : Zn = $\sim 8.5 : 1$, typical for ZIF-8 formation.

Zif-8-Au: First, we dissolved 3 g of hexahydrate zinc nitrate from Merck in 200 mL of methanol (solution 1). Then, we dissolved 6 g of 2-methylimidazole (MIM) in 200 cc of water (solution 2). 500 cc of gold salt solution (100 ppm) was stirred in a cool water bath at a temperature below 25 degrees. Now, the MIM solution was gradually added to the beaker containing the gold salt, and immediately, the zinc nitrate solution was added to the reaction vessel and stirred in a cool water bath for one hour. 0.01 M $NaBH_4$ solution

was added to the system. The sample was centrifuged after 48 hours and then dried, known as Zif-8-Au. Molar ratio: Zn : Au $\approx$ 10 mmol : 0.00254 mmol $\approx$ 3940 : 1
Zif-8-Fe: First, we dissolved 3 g of hexahydrate zinc nitrate in 200 mL of methanol (solution 1). Next, we add 0.2 g of nano iron oxide to 60 mL of methanol and stir until it is dissolved (solution 2). Then, solution 2 was added to solution 1 and stirred for 2 hours. Then, we dissolved 7 g of MIM in 200 cc of methanol (solution 3). Then, we quickly added the resulting mixture from $1+2$ to solution 3 and stirred for one hour. Then, the solution was filtered, washed with methanol, and the precipitate was collected, known as Zif-8-Fe_3O_4 and labeled Zif-8-Fe. Molar ratio: Zn : Fe $\approx$ 10 mmol : 2.58 mmol $\approx$ 3.9 : 1

2.3 Drug loading

The synthesis of flutamide-loaded ZIF-8 nanoparticles was achieved via in situ encapsulation, where the drug was present during MOF formation. To synthesize flutamid@Zif-8, it involved dissolving 3 g of zinc nitrate hexahydrate in 200 mL of methanol and 7 g of MIM in 100 mL of methanol. The zinc solution was then added at once to the MIM solution. A 200 mL solution of 30 ppm flutamide was subsequently added to the reaction mixture, which was stirred for 2 h before the precipitate was collected by centrifugation. To prepare flutamide@Zif-8-Au, a similar method was employed. This method involved dissolving 3 g of zinc nitrate hexahydrate in 200 mL of methanol and 7 g of MIM in 200 mL of water at 25 °C. A 500 mL solution of 100 ppm Au salt was stirred in a cool water bath below 25 °C. The MIM solution was gradually added to the gold salt (gold sodium chloride), followed immediately by the zinc nitrate solution. This was stirred for one hour with a 200 mL solution of 30 ppm flutamide (at 250 °C). The sample was centrifuged after 48 h and then dried in an oven. Synthesizing flutamide@Zif-8-Fe began by dissolving 5.86 g of zinc nitrate hexahydrate in 200 mL of methanol and 0.2 g of iron oxide in 60 mL of methanol. This iron oxide solution was added to the zinc nitrate solution and stirred for one hour. The resulting mixture was then rapidly added to a solution of 12.96 g of MIM in 200 mL of methanol, along with a 200 mL solution of 30 ppm flutamide. This final mixture was stirred for two hours, followed by filtration, washing with methanol, and collection of the precipitate.

2.4 SEM and EDX

The morphology and surface roughness of the nanoparticles were characterized using a scanning electron microscope (SEM). The FEI Quanta 200 SEM was operated at an accelerating voltage of 25 kV, which was chosen to balance resolution with a high signal-to-noise ratio. Before imaging, the non-conductive samples were coated with a thin layer of gold to create a conductive surface.

2.5 FTIR

FT-IR spectroscopy was employed to study the chemical composition and structure of the samples. The analysis was performed using a JASCO-4600 spectrophotometer, which is a powerful mid-infrared spectrometer. The specific spectra were captured in the 4000-400 cm^{-1} region. This range is significant as it covers the mid-infrared region, which is ideal for studying fundamental molecular vibrations and provides a unique "molecular fingerprint" of the material.

2.6 XRD

The crystallinity of the samples was assessed using X-ray diffraction (XRD), a non-destructive technique that analyzes the atomic structure of materials. The analysis was performed with an EQuniox 300 diffractometer using Cu-Kα radiation. Measurements were performed over a 2θ range of $10-70°$, which allows for the examination of both surface-level and deeper structural characteristics of the material.

2.7 BET

The specific surface area, pore volume, and pore diameter of the decellularized and modified hydrogel stems were evaluated using nitrogen adsorption isotherms, a technique based on the Brunauer-Emmett-Teller (BET) method. This analysis was conducted using a BELSORP MINI II instrument. Before the analysis, the samples were heated to 100 °C for one hour in order to eliminate any residual gases and moisture, a crucial step for obtaining accurate results. The BET method itself calculates the surface area based on the quantity of gas molecules that form a single layer on the solid surface, with nitrogen gas typically used for this purpose.

2.8 Drug release

100 mg of flutamide-loaded nanoparticles (drug loading: 142, 72, and 188 µg/g for ZIF-8, ZIF-8-Au, and ZIF-8-Fe, respectively) was placed in an activated dialysis bag and immersed in 50 mL of distilled water. At predetermined intervals (1, 8, 20, 32, 44, 64, and 76 h), 4 mL of the medium was withdrawn for analysis and immediately returned. Absorbance was measured at 240 nm, and each experiment was performed in triplicate.
Sink conditions were maintained because the maximum drug amount in the nanoparticles (0.0072–0.0188 mg) is far below the solubility limit of flutamide in water ($\sim$ 10 mg in 50 mL), ensuring accurate measurement of release kinetics.

2.9 Kinetic study

The kinetic release of the drug from the nanoparticles was analyzed using several numerical kinetic models. The models employed in this study were the Higuchi, Korsmeyer-Peppas, zero-order, and first-order models, which are commonly used to describe and predict drug release mechanisms from a matrix.

2.10 Statistical analysis

The data were statistically analyzed using Prism software, with ANOVA tests to determine significance. All results were presented as the mean $\pm$ standard deviation, and a statistical significance threshold was set at $P < 0.05$.

3. Results and discussion

MOFs, particularly Zif-8 nanoparticles, have garnered significant attention in biomedical applications due to their

high porosity and exceptional drug loading capacity. However, ongoing research continues to explore methods for further enhancing their performance for targeted delivery. Ion-doping has emerged as a promising strategy to modify the framework's properties and improve its encapsulation efficiency. In this study, we employed this approach by incorporating gold (Au) and iron oxide (Fe_3O_4) into the Zif-8 structure. The primary objective of this modification was to enhance the loading capacity and functional properties of the nanoparticles for the targeted delivery of Flutamide.

The choice to dope Zif-8 with Fe and Au stems from the need to fine-tune its structure and behavior in ways that pure Zif-8 alone cannot offer. When Fe^{3+} ions are introduced into the Zif-8 framework, they can partially replace Zn^{2+} or interact with the imidazolate linkers. This creates slight distortions in the structure, small changes in crystallinity and pore openings, that increase the number of defects inside the framework. These defects are beneficial because they change the pore environment and create new sites where drug molecules can interact more strongly. For a hydrophobic drug like Flutamide, this more varied and slightly more polar microenvironment can improve its adsorption and retention within the carrier (Quintero-Álvarez et al., 2022).

Au doping contributes in a different but complementary way. Very small Au nanoparticles or clusters can become incorporated into or attached to the Zif-8 matrix, altering the pore texture and increasing the available surface area. Their presence adds extra surface roughness and can strengthen interactions with aromatic drugs through $\pi - \pi$ and other weak intermolecular forces. Au has also been shown to influence the stability of Zif-8, helping the material resist premature breakdown at physiological pH while still allowing it to respond to acidic conditions typically found in tumor tissues (He et al., 2024). Flutamide is an antiandrogen drug used against androgen-sensitive cancer cells. The incorporation of Fe and Au ions in the nanocarriers may provide additional therapeutic benefits by modulating oxidative stress or intracellular signaling pathways, which could potentially act synergistically with Flutamide. Although the current study focused on cytotoxicity and drug delivery efficiency, these interactions highlight a promising avenue for enhancing anticancer efficacy and warrant further experimental investigation (Koch et al., 2015).

SEM images of the pure Zif-8 nanoparticles (Fig. 1 a) show they are largely homogeneous and multifaced, with a somewhat spherical shape. While the size distribution is relatively uniform, a few larger particles are also present within the sample. The mean diameter is equal to 50-70 nm. These results were in line with the previous study done by Daniel et al. (Eiras et al., 2016). After Au doping, Au-doped Zif-8 Nanoparticles did not show a significant difference compared to Zif-8 (Fig. 1 b). The mean diameter was equal to 50-80 nm, which shows a bit of enhancement in particle size that can be attributed to the Au doping. After Au doping, the particles look more multifaceted and spherical. It was reported that more calcination causes a more spherical geometry can be attributed to the calcination process (Chang et al., 2019). Interestingly, after doping Fe_3O_4 in Zif-8, a new geometry can be observed (Fig. 1 c). Fully multifaceted nanoparticles were generated with a mean diameter of about 500 nm. Obviously, there is a significant enhancement in particle size, but with a new dimension and structure. These results were in line with the previous study (Jiang et al., 2015).

Figure 2 demonstrates the results of EDX for all particles, including Zif-8, Au-doped Zif-8, and Fe_3O_4-doped Zif-8. Az can be seen that all images confirm the presence of Zn. Fig. 2 b shows 36% and 58% of Zn and Au, respectively. Also, Fig. 2 c shows about 25% and 10% of Zn and Fe, respectively. These results confirm that the synthesis was done successfully.

The Fourier-Transform Infrared (FTIR) spectrum of pure Zif-8 was analyzed to confirm the successful formation and structural integrity of the framework (Fig. 3). The spectrum is defined by the characteristic vibrational modes of the 2-methylimidazole linker and the Zn-N coordination bond. Prominent peaks at approximately 3135 cm^{-1} and 2930 cm^{-1} are attributed to the aromatic and aliphatic C–H stretching vibrations, respectively (Hu et al., 2011). Additionally, peaks corresponding to the imidazole ring stretching modes appear between 1580-1600 cm^{-1} (C=N and C=C bonds) and 1300–1500 cm^{-1} (C–N stretching) (Hu et al., 2013). Crucially, the presence of a characteristic low-frequency peak at 425 cm^{-1}, assigned to the Zn–N bond stretching vibration, definitively confirms the formation of the Zif-8 framework. Gold-doped Zif-8 (Au-Zif-8) has a very similar FTIR spectrum to pure Zif-8, but with some key differences that confirm the successful incorporation of gold nanoparticles without disrupting the main framework. The primary goal of an FTIR analysis for Au-Zif-8 is to verify that the core Zif-8 structure remains intact. The FTIR spectrum of an Fe_3O_4-Zif-8 composite is characterized by the coexistence of both the Zif-8 framework's signature peaks and the distinctive absorption band of iron oxide. The presence of peaks for aromatic C-H stretching (around 3135 cm^{-1}), aliphatic C-H stretching (around 2930 cm^{-1}), and most importantly, the Zn-N bond (around 425 cm^{-1}) confirms that the Zif-8 structure remains intact (He et al., 2024). Furthermore, a strong absorption band typically appears between 500 and 600 cm^{-1}, corresponding to the Fe-O bond stretching vibration, which serves as definitive evidence of the successful incorporation of Fe_3O_4 nanoparticles into the composite (Xu et al., 2021).

The XRD pattern of a successfully synthesized Zif-8 was highly crystalline, meaning it had sharp, well-defined peaks at specific diffraction angles (2θ) (Fig. 4). The presence of these sharp peaks confirmed the formation of the Zif-8 sodalite (SOD) topology. The most important peaks were at approximately 7.3°, 10.3°, 12.7°, 14.7°, 16.4°, and 17.9°, which confirmed the successful synthesis of Zif-8 crystal (Kida et al., 2013). For an Au-Zif-8 composite, the XRD pattern should be a combination of two distinct sets of peaks, which confirms a successful composite material. First, all of the characteristic Zif-8 peaks were present (with a shift) to show that the framework's structure remained intact after the gold doping process. Second, new sharp peaks corresponding to the face-centered cubic (FCC) structure of crystalline gold were also observed. The main gold peaks

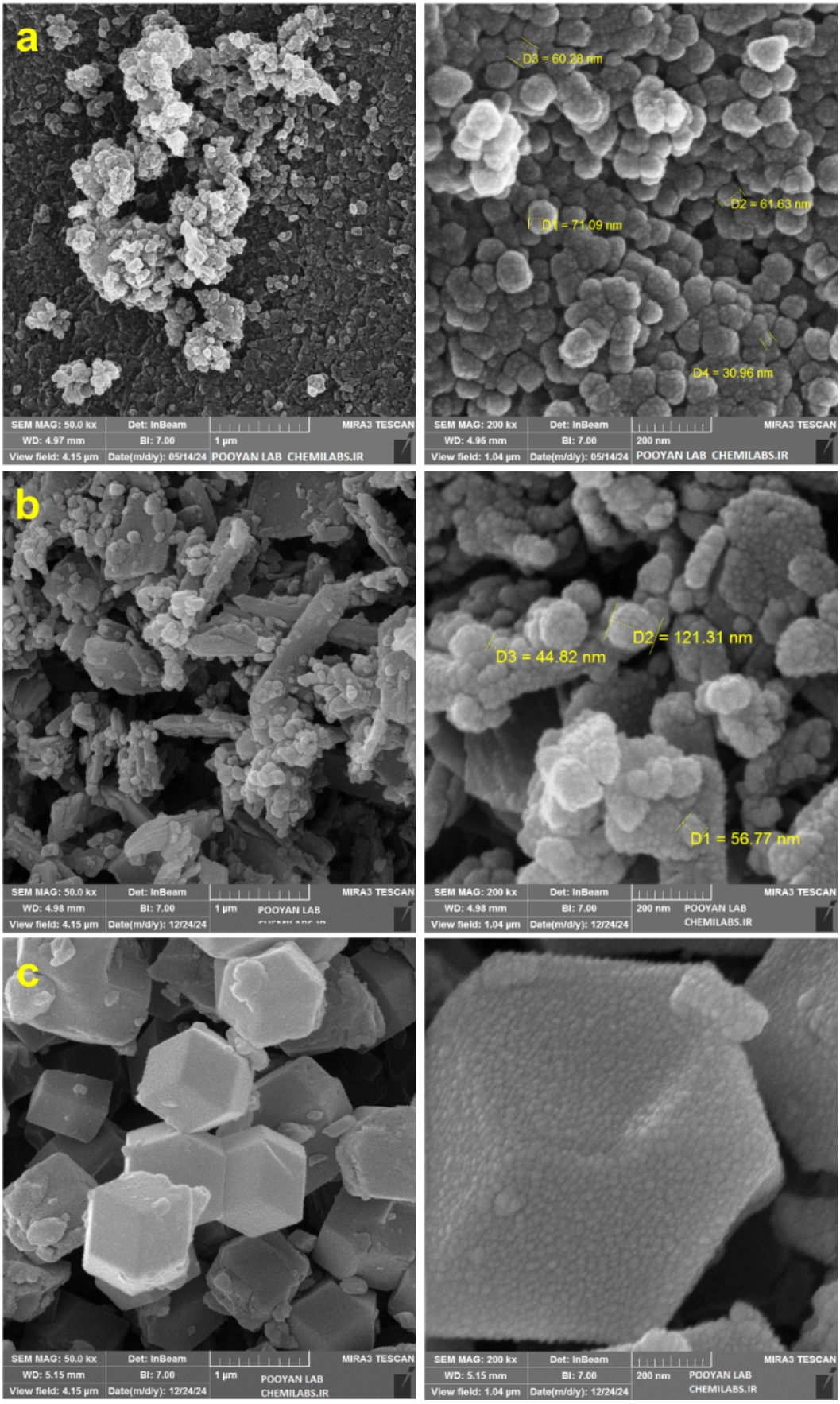

Figure 1. Results of SEM for a: Zif-8, b: Au-doped Zif-8, and c: Fe_3O_4-doped Zif-8. Scale bar (left: 1 µm and right: 200 nm).

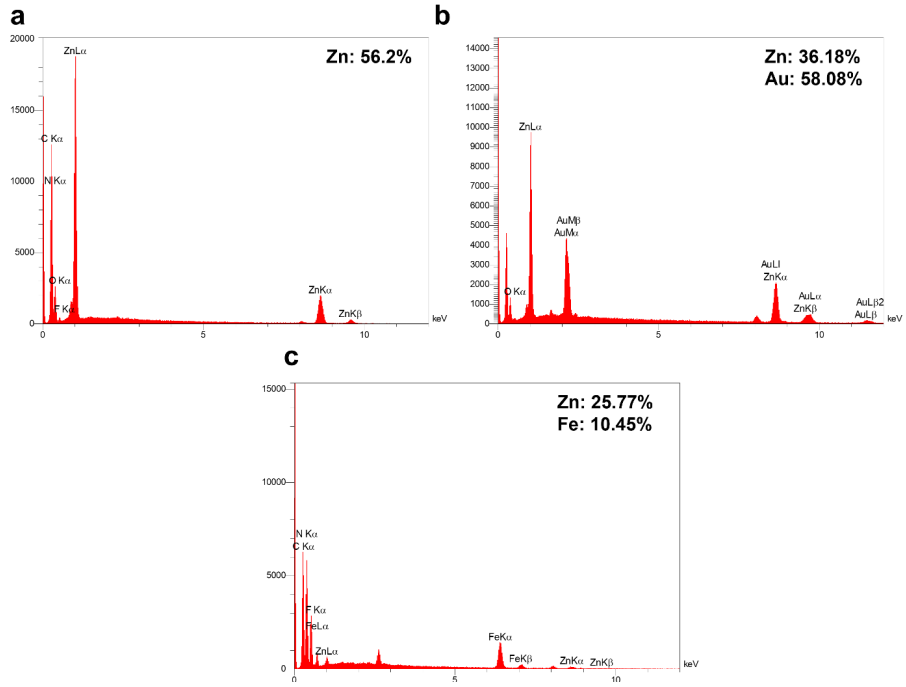

Figure 2. Results of EDX for a: Zif-8, b: Au-doped Zif-8, and c: Fe_3O_4-doped Zif-8.

were at approximately 38.9° (111 plane) and 43.6° (200 plane) (Kang et al., 2021). The coexistence of both the Zif-8 and gold peaks is the definitive evidence of the successful composite formation. Similarly, the XRD pattern for the Fe_3O_4-Zif-8 composite displayed peaks from both components. The integrity of the Zif-8 framework was confirmed by the presence of its characteristic peaks (at 7.3°, 10.3°, etc.) as previously described. In addition, new, sharp peaks appeared that match the standard pattern for crystalline magnetite (Fe_3O_4). The main peaks for magnetite were typically found at approximately 29.3°, 30.1°, 36°, 36.9°, 53.4°, and 57.0° (Xu et al., 2021). The presence of both the Zif-8 peaks and the distinct magnetite peaks is the definitive proof of a successful magnetic composite material. The relative intensity of these two sets of peaks can also provide a rough estimation of the Fe_3O_4 loading ratio within the composite.

The observed shifts in the characteristic Zif-8 peaks within the XRD pattern are a significant finding. Unlike simple physical mixtures, which show no peak shifts, these changes indicate that the interplanar spacing of the Zif-8 crystal has been altered (J. Yang, 2014). This is strong evidence that the dopant ions were successfully incorporated into the Zif-8 lattice, likely by substituting for the central zinc ions. This confirms a more fundamental interaction than simple surface deposition and validates the successful synthesis of a doped crystal structure (Liu and Wöll, 2017). This key finding should be highlighted as it provides crucial insight into the morphology and properties of the new composite material.

To sum up, the XRD patterns of the doped samples show slight shifts in the main diffraction peaks relative to the pristine MOF, indicating substitutional incorporation of Fe and Au ions into the lattice. Additionally, minor extra peaks

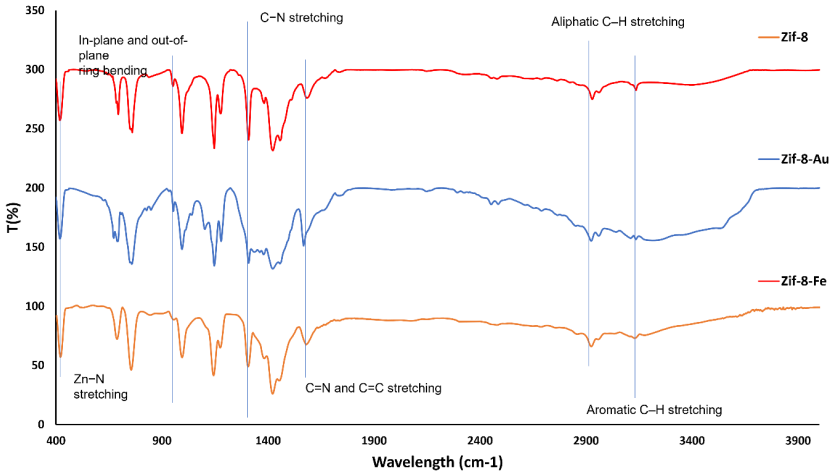

Figure 3. Results of FTIR for a: Zif-8, b: Au-doped Zif-8, and c: Fe_3O_4-doped Zif-8.

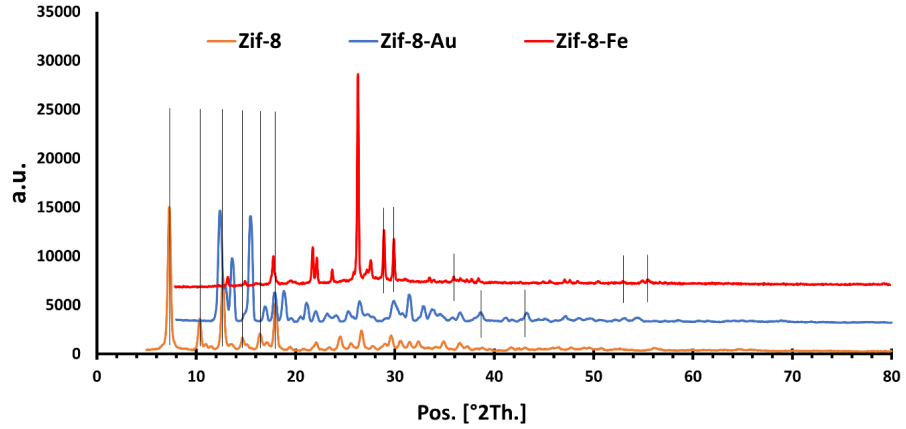

Figure 4. Results of XRD for a: Zif-8, b: Au-doped Zif-8, and c: Fe_3O_4-doped Zif-8.

in the Au-doped sample suggest possible surface species or small clusters. Peak broadening further supports lattice strain induced by doping.

The BET surface area (SBET) values for the materials were measured as 1415.5 m^2/g for pure Zif-8, 553.57 m^2/g for Zif-8-Au, and 2676.3 m^2/g for Zif-8-Fe (Table 1) that which showed a significant difference compared to each other ($P < 0.01$). The total pore volume of Zif-8, Zif-8-Au, and Zif-8-Fe were 0.54 cm^3/g, 0.26 cm^3/g, and 1.0 cm^3/g, respectively showing a significant difference ($P < 0.01$). The mean pore diameters were determined to be 1.53 nm (Zif-8), 1.89 nm (Zif-8-Au), and 1.50 nm (Zif-8-Fe_3O_4). No significant difference between Zif-8 and Zif-8-Fe ($P > 0.05$).

The significant decrease in both the surface area and pore volume of the Zif-8-Au composite compared to the pure Zif-8 is expected and is strong evidence of a successful synthesis. The gold nanoparticles, when incorporated, occupy a portion of the Zif-8's intrinsic pores, effectively blocking access to them and causing the observed reduction in porosity (Jiang et al., 2009). The slight increase in the mean pore diameter, as shown in SEM images, suggests that the gold particles may have slightly altered the pore structure, possibly creating larger, less uniform channels, or that the analysis is dominated by the remaining open, larger pores (Lu et al., 2020). The substantial increase in both the surface area and total pore volume of the Zif-8-Fe composite is an interesting and important finding. This suggests that the iron oxide nanoparticles are not just encapsulated within the existing Zif-8 pores but are also introducing additional, new pore structures (Jiang et al., 2009). The slight decrease in the mean pore diameter compared to pure Zif-8 suggests that these new pores are likely micropores formed either within the iron oxide itself or at the interface between the Zif-8 and Fe nanoparticles (Li et al., 2023). This unique result is worth highlighting as it could lead to enhanced performance in applications like gas storage or catalysis, where increased porosity is beneficial.

Up to now, the synthesis of ion-doped nanoparticles has been confirmed, and their characteristics have been studied. In the rest, these nanoparticles were nominated for flutamide loading and their release. Based on the results, drug loading capacity for Zif-8, Zif-8-Au, and Zif-8-Fe was 14.2, 7.2, and 18.8 mg/g of nanoparticle, respectively. The drug loading capacity results were in direct correlation with the BET analysis findings. The highest drug loading capacity was achieved with the Zif-8-Fe composite, a result that directly corresponds to its enhanced total pore volume. Conversely, the Zif-8-Au composite exhibited the lowest capacity, which is consistent with the observed reduction in its total pore volume compared to pure Zif-8. Consequently, the drug loading capacity of the MOF can be either increased or decreased depending on the chosen doping ion and its effect on the material's porosity.

Figure 5 shows the flutamide release diagram from Zif-8, Zif-8-Au, and Zif-8-Fe. As can be seen, higher release belonged to Zif-8-Fe, and the reason is justified by the higher loading capacity. However, the release rate for Zif-8-Fe was slower by showing a gentler slope. The slower release can be attributed to the unique changes in the material's porous structure and potential interactions with the Fe_3O_4 nanoparticles, as evidenced by previous BET analysis and XRD data. While BET data showed an increase in total pore volume, the mean pore diameter was slightly smaller. This suggests that the Fe_3O_4 nanoparticles likely created new, smaller pores or a more tortuous (winding) path for the drug molecules to diffuse through (Proenza and Longo,

Table 1. Results of BET analysis for a: Zif-8, b: Au-doped Zif-8, and c: Fe_3O_4-doped Zif-8.

Parameters	Zif-8	Zif-8-Au	Zif-8-Fe
$a_{s,BET}$ (m^2/g)	1415.5[a]	553.57[b]	2676.3[c]
Total pore volume ($p/p_0 = 0.990$) (cm^3/g)	0.54[a]	0.26[b]	1[c]
Mean pore diameter (nm)	1.53[a]	1.89[b]	1.5[a]

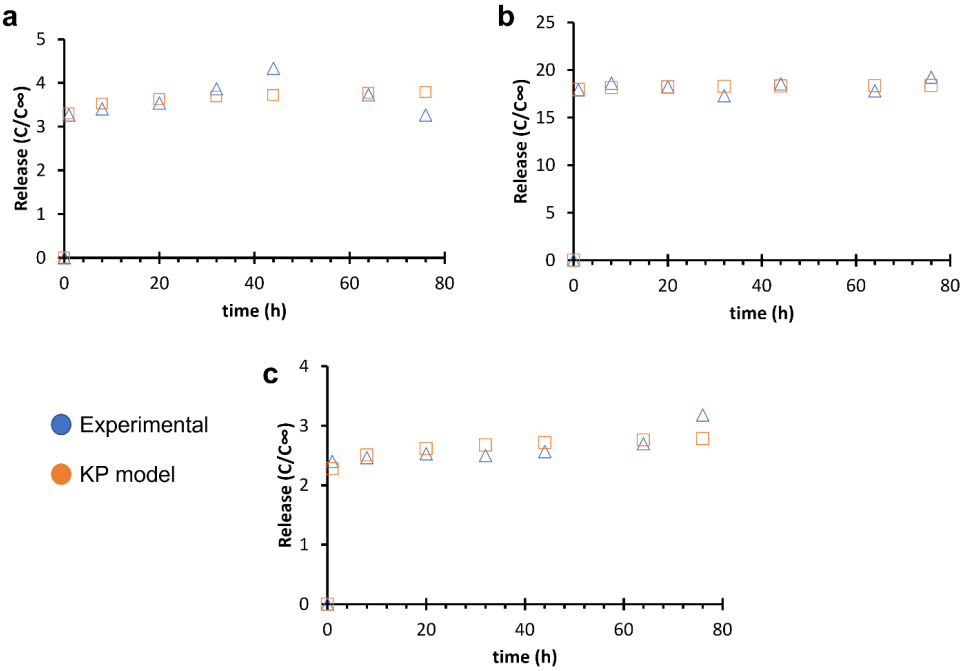

Figure 5. Experimental results and modeling data for flutamide release from a: Zif-8, b: Au-doped Zif-8, and c: Fe_3O_4-doped Zif-8.

2019). A more complex and winding pathway significantly slows down the release process (Lei et al., 2020). The presence of the Fe_3O_4 nanoparticles may be creating new or stronger binding sites for the drug. The surface of the iron oxide could be interacting chemically or physically with the flutamide molecules, causing them to be held more tightly within the composite. This stronger interaction requires more time and energy to break, resulting in a prolonged and slower release (Baljon et al., 2004; Deac et al., 2022).

Release data for Zif-8-Au showed low but faster release of flutamide. The significant reduction in the total pore volume for Zif-8-Au indicated that the gold nanoparticles occupied a large portion of Zif-8's internal pores. This physically limited the amount of Flutamide that could be loaded into the material, leading to a low total capacity. The rapid release rate suggests that the loaded drug was primarily located on the surface of the composite or in the most easily accessible pores (Liu et al., 2007). Since the internal pores were largely blocked by the gold ion, it seems that the drug was not trapped deep within the Zif-8 framework. Once the material was placed in the release medium, the drug quickly diffused from these surface locations, resulting in a steep slope and a fast release (Palvai et al., 2024).

In conclusion, the gold doping fundamentally changed the material's morphology. It reduced the total available space for drug loading but, more importantly, altered the internal pore structure, forcing the drug to reside in external locations where it could be released rapidly (Senjković and Jalšenjak, 1981). This finding is a crucial insight into how different doping agents can control both the capacity and release kinetics of MOF-based drug delivery systems.

Release from Zif-8 was similar to Zif-8-Fe. It indicates that both materials follow the same diffusion-controlled release mechanism, with the slight difference highlighting the successful modification of the Zif-8 framework by the iron oxide dopant. The release from pure Zif-8 is a classic example of diffusion from a highly porous, uniform network (Wang et al., 2024). Its well-defined, intrinsic pores allow drug molecules to diffuse out along a relatively predictable path, leading to a consistent release rate.

To distinguish these differences in release, a kinetic study was performed using zero-order, first-order, Higuchi, and Korsmeyer-Peppas (KP) models. These models are widely used and highly relevant for studying the release kinetics from porous nanoparticles (Khorshidian et al., 2024; Esmaeili et al., 2023; Dash, 2010). Each model provides a unique mathematical framework for understanding and describing the underlying release mechanism. Table 2 shows the appropriate results for these models. The Korsmeyer–Peppas model, in particular, provides the diffusion exponent (n value), which indicates the dominant release mechanism. For cylindrical systems, an n value ≤ 0.45 suggests Fickian diffusion, $0.45 < n < 0.89$ indicates anomalous or non-Fickian transport (a combination of diffusion and matrix relaxation), and $n \geq 0.89$ corresponds to Case-II transport, typically governed by polymer swelling or erosion. By comparing the n values obtained for our samples, we could distinguish whether drug release was primarily diffusion-controlled or involved additional mechanisms such as polymer relaxation or matrix degradation. Furthermore, differences among the fitted models highlight how each one captures specific aspects of the release process: First-order and Second-order models describe concentration-dependent kinetics, the Higuchi model assumes diffusion from a homogeneous matrix, and the Korsmeyer–Peppas model offers a more general description for systems where multiple mechanisms coexist. Together, these analyses provide a comprehensive understanding of how structural and compositional factors influence the release behavior of the formulation (Khorshidian et al., 2024;

Table 2. The obtained results for the considered models for numerical modeling.

Groups	Parameters	Zero order $F = kt$	First order $F = \exp(-Kt)$	Korsmeyer-Peppas $F = kt^n$	Higuchi $F = kt^{0.05}$
Zif-8	k	0.06	0	3.3	0.56
	n	-	-	0.03	0.5
	R^2	0.46	NA	0.97	0.65
Zif-8-Au	k	0.33	0	17.95	2.79
	n	-	-	0.01	0.5
	R^2	0.45	NA	1	0.61
Zif-8-Fe	k	0.05	0	2.28	0.41
	n	-	-	0.05	-
	R^2	0.61^a	NA	0.98^b	0.73^a

*$F = C/C_\infty$, C: flutamide concentration at t, C_∞: total concentration of flutamide
a,b,c: different letters mean a significant difference.

Esmaeili et al., 2023).

The kinetic analysis of flutamide release from Zif-8, Zif-8-Au, and Zif-8-Fe demonstrates that the different mathematical models describe the release behavior with varying accuracy. The zero-order model showed relatively low correlation coefficients ($R^2 = 0.45 - 0.61$), indicating that none of the samples followed a constant-rate release profile. Although Zif-8-Fe presented a slightly higher R^2 compared to the other groups, the overall fit remained weak, confirming that zero-order kinetics is not an appropriate descriptor for these systems. Similarly, the first-order model did not describe the release behavior at all; the fitting returned $k = 0$ with no meaningful correlation values, demonstrating that the release was not concentration-dependent. This confirms that flutamide does not diffuse out of the MOFs based on a typical dissolution-driven mechanism.

In contrast, the Korsmeyer–Peppas model provided an excellent fit for all three samples, with R^2 values ranging from 0.97 to 1.00. This strong correlation indicates that this model is the most suitable for describing the release behavior of flutamide from the ZIF-8-based composites (Esmaeili et al., 2024). The release exponent (n) values for all samples were extremely low ($0.01 - 0.05$), pointing to a purely Fickian diffusion mechanism dominated by an immediate burst-release phase rather than a controlled or sustained release. Among the materials, Zif-8-Au exhibited the highest release rate constant ($k = 17.95$), indicating the fastest overall release, while Zif-8 and Zif-8-Fe showed lower constants, though still within the burst-release range. The Higuchi model, which typically describes diffusion from porous matrices, showed only moderate fitting quality, with R^2 values between 0.61 and 0.73. This suggests that although diffusion contributes to the release behavior, the Higuchi model alone cannot accurately capture the system's kinetics. Taken together, the results confirm that the flutamide release from these MOFs is dominated by Fickian diffusion with a strong initial burst effect. Doping ZIF-8 with Au or Fe does not introduce sustained-release characteristics; instead, Au doping enhances the release rate even further (Talevi and Ruiz, 2022). Overall, these findings demonstrate that none of the studied materials provide meaningful sustained release, and future modifications should focus on strengthening drug–carrier interactions or introducing diffusion-barrier structures to reduce the burst release and achieve more controlled delivery.

However, Machine learning (ML) offers a promising approach for optimizing nanocarrier design, including tuning Fe and Au ion doping levels to achieve tailored drug release profiles. By integrating experimental data with predictive ML models, future studies could efficiently identify optimal synthesis conditions and release kinetics, thereby enhancing the therapeutic performance of these nanocarriers. Incorporating such strategies could significantly expand the applicability and precision of ZIF-8-based drug delivery systems.

Table 3 provides a comparative overview of different nanocarrier systems previously reported for flutamide delivery, highlighting their encapsulation efficiency (EE%), drug loading (DL%), particle size, release behavior, and key advantages. This comparison helps position the ZIF-8–based MOFs relative to established delivery systems and shows how the ion-doped ZIF materials differ in terms of performance and potential application.

Solid lipid nanoparticles (SLNs) typically show moderate encapsulation efficiency (around 65%) and very low drug loading ($\sim 3.27\%$) (Hamishehkar et al., 2016). Their particle size is approximately 198 nm, and their release behavior is not always clearly described in the literature, although some formulations demonstrate stability over extended storage times. While SLNs are known for good stability and biocompatibility, their limited drug loading restricts their usefulness for drugs requiring higher payloads. Polymeric micelles, particularly PAM–PA micelles, demonstrate significantly higher encapsulation efficiency ($\sim 94.5\%$) and improved drug loading ($\sim 48.6\%$ for optimized formulations) (Mirsafaei and Varshosaz, 2020). Their particle size is smaller, around 88 nm, and their release profile is strongly pH-responsive, showing nearly complete release under acidic conditions and controlled release at physiological pH. These characteristics make polymeric micelles highly effective for targeted or environment-responsive delivery.

Nanostructured lipid carriers (NLCs) offer one of the high-

Table 3. Comparison table with recent literature on Flutamide nanocarriers.

Nanocarrier type	EE (%)	DL (%)	Particle size	Release Kinetics/ Profile	Key Advantages/ Notes	Ref.
Solid Lipid Nanoparticles (SLNs) (e.g., flutamide SLNs)	∼ 65%	∼ 3.27%	∼ 198 nm	Not always detailed; stable over 2 months in some studies	Good stability, well-known formulation, but limited loading	(Hamishehkar et al., 2016)
Polymeric Micelles (PAM–PA micelles)	∼ 94.5%	∼ 48.6% (for optimal ratio)	∼ 88 nm	∼ 85.6% release in 10 h at pH 7.4; full release at pH 4.5	Very high loading, pH-responsive release	(Mirsafaei and Varshosaz, 2020)
Nanostructured Lipid Carriers (NLCs)	∼ 97.7%	Not always reported or low	(from TEM/SEM), optimized NLCs (size not always in abstract)	∼ 88% release; follows Korsmeyer–Peppas kinetics	Very high EE, good release, lipid biocompatibility	(Sabale et al., 2024)
Cholesterol-based Nanovesicles / Niosomes	∼ 72.8%	Not always clearly reported in %, but implied from other data	∼ 748.6 nm	∼ 72.2% release in 24 h	Enhanced bioavailability, *in vivo* data, *ex vivo* intestinal absorption	(Ali et al., 2021)
Casein (protein) Micelles	Not in % EE in some reports, but good encapsulation	Not always DL reported	$<$ 100 nm	Sustained release up to $\approx$ 5 days *in vitro*	Very biocompatible, *in vivo* efficacy, and reduced hepatotoxicity	(Elzoghby et al., 2013)
(Zif 8 Fe/Au MOF)	ZIF-8 (23.7%), ZIF-8-Au (12.0%), ZIF-8-Fe (31.3%)	ZIF-8 (14.20 mg/g), ZIF-8-Au(7.20 mg/g), ZIF-8-Fe (18.80 mg/g)	50-500 nm	Your release profile (e.g., % over time, kinetics)	Tunable release via ion doping; strong structural stability; potential for high loading and controlled delivery	Our work

est encapsulation efficiencies (∼ 97.7%) among lipid-based systems (Sabale et al., 2024). However, drug loading values are not consistently reported. Their release profiles often fit Korsmeyer–Peppas diffusion kinetics, indicating controlled release behavior. NLCs are attractive due to lipid biocompatibility, high stability, and high encapsulation capacities. Cholesterol-based nanovesicles or niosomes typically show EE values around 72.8% with particle sizes near 748 nm (Ali et al., 2021). Their release behavior generally reaches 72% within 24 hours. While larger in size, they are recognized for improved bioavailability, intestinal absorption, and promising in vivo performance. Casein micelles do not always report EE% or DL% clearly, yet they are known to encapsulate hydrophobic molecules effectively. Their particle sizes remain below 100 nm, and they can sustain release for several days (Elzoghby et al., 2013). Their natural biocompatibility, low toxicity, and suitability for oral or injectable delivery make them advantageous for chronic administration models.

The final row situates the ZIF-8, ZIF-8-Au, and ZIF-8-Fe MOFs in our study within this landscape. These materials show drug loading capacities ranging from 7.2 mg/g to 31.3 mg/g, depending on the metal dopant, with the Fe-doped version achieving the highest DL. Unlike lipid and polymer systems, the ZIF-based materials are distinguished by their tunable release behavior via ion doping and their high structural stability. While traditional nanocarriers rely on soft or semi-soft matrices, ZIFs offer a rigid, porous framework that can be chemically modified to tailor interactions with the drug. The release kinetics observed in the current work, particularly the Fickian diffusion profile and burst-release behavior, highlight potential for further optimization. Overall, the table demonstrates that ZIF-based MOFs offer competitive drug loading and a unique platform for chemically tunable release, but they require additional engineering to match the sustained-release performance of casein micelles or the extremely high encapsulation of NLCs.

4. Conclusion and future perspective

In this study, a series of novel Zif-8–based composites (Zif-8, Zif-8-Au, and Zif-8-Fe) was successfully synthesized through ion doping, demonstrating an effective and versatile strategy for tailoring the physicochemical properties of metal–organic frameworks. Structural analyses using XRD and FTIR confirmed the formation of the Zif-8 crystalline network and the successful incorporation of Au and Fe_3O_4 nanoparticles. The observed shifts in XRD peak positions further provided evidence of dopant ions interacting with and partially integrating into the Zif-8 lattice structure, thereby altering its crystallinity and pore characteristics. BET surface area measurements revealed distinct effects from each dopant: While Au doping significantly reduced surface area and pore volume, likely due to partial pore blocking, Fe_3O_4 doping enhanced both parameters, suggesting improved pore accessibility and structural expansion.

These structural modifications directly translated into notable differences in drug delivery behavior. The Zif-8-Fe composite exhibited the highest drug loading capacity and a prolonged, controlled release pattern, which can be attributed to its increased porosity, modified pore tortuosity, and enhanced surface–drug interactions. In contrast,

Zif-8-Au displayed reduced loading efficiency and a rapid, low-capacity release profile, consistent with its more compact structure and limited accessible pores. Kinetic analysis using the Korsmeyer–Peppas model indicated that all composites followed a Fickian diffusion release mechanism, highlighting the stability and predictability of their drug release processes. Collectively, these findings confirm that ion doping is a powerful tool for fine-tuning porosity, diffusion pathways, and release kinetics in MOF-based carriers.

The hydrolytic stability of ZIF-8 is a critical factor for its application as a drug delivery system under physiological conditions. In this study, the stability was enhanced through Fe and Au doping, and XRD analysis confirmed that the material maintained its structural integrity during the 48–72 hour drug release experiments at neutral pH. These results indicate that the nanocarriers are sufficiently robust for sustained drug delivery in near-physiological environments. This work opens several promising directions for further research. First, systematic exploration of different dopant ions, including biometals such as Zn^{2+}, Ca^{2+}, Cu^{2+}, and Co^{2+}, may yield composites with customized therapeutic responses, magnetic properties, or catalytic behavior. Second, integrating stimuli-responsive components (pH-, temperature-, or redox-sensitive dopants) could enable smart drug delivery systems capable of targeted release within specific pathological microenvironments, such as tumors or infected tissues. Third, expanding this strategy to other MOF families may generalize the doping approach for a broader range of biomedical and diagnostic applications. Finally, future in-vitro and in-vivo biological evaluations, including cytotoxicity assays, cellular uptake studies, and biodistribution analyses, will be critical for translating these materials into clinically relevant drug delivery platforms. Overall, this study establishes a strong foundation for designing next-generation MOF-based therapeutics with precisely engineered structural and functional properties.

Although the current study focused on the initial assessment of the proposed nanocarriers, further investigations are warranted to better understand their cellular interactions. In particular, the effect of Fe and Au doping on the mechanism of cellular uptake remains to be elucidated. Future studies using fluorescence-labeled drugs or nanocarriers, combined with microscopy techniques, could clarify whether these materials are internalized via endocytosis, direct membrane fusion, or other pathways. Such insights will provide a more comprehensive understanding of the nanocarrier behavior and enhance the design of safe and effective drug delivery systems.

Last but not least, a major limitation of the current study is the lack of *in vivo* or *ex vivo* experiments, which are essential to fully assess the bioavailability, pharmacokinetics, and safety of the ZIF-8-Fe/Au nanocarriers for Flutamide delivery. Future work will focus on conducting such studies to validate the therapeutic potential and biocompatibility of the system under physiological conditions.

Acknowledgment

We are grateful to Islamic Azad University for providing the resources and facilities necessary for conducting this research.

Authors contributions

All authors contributed equally to the conception, design, execution, and writing of this work. All authors read and approved the final manuscript.

Availability of data and materials

The datasets generated during and/or analyzed during the current study are available from the corresponding author on reasonable request.

Conflict of interests

The authors declare that they have no known competing financial interests or personal relationships that could have appeared to influence the work reported in this paper.

References

Ali M. A., Mohamed M. I., Megahed M. A., Abdelghany T. M., El-Say K. M. (2021) Cholesterol-Based Nanovesicles Enhance the In Vitro Cytotoxicity, Ex Vivo Intestinal Absorption, and In Vivo Bioavailability of Flutamide. *Pharmaceutics* 13 (11)

Baljon A. R., Vorselaars J., Depuy T. J. (2004) Computational studies of contact time dependence of adhesive energy due to redistribution of the locations of strong specific interfacial interactions. *Macromolecules* 37 (15): 5800–5806.

Bao G., Mitragotri S., Tong S. (2013) Multifunctional nanoparticles for drug delivery and molecular imaging. *Annual Review of Biomedical Engineering* 15 (1): 253–282.

Bhardwaj A. K., Kant A., Rehalia A., Singh V., Sharma R. (2023) A review on nanomaterials for drug delivery systems and application of carbon based nanomaterials. *ES Materials & Manufacturing* 21 (2): 824.

Chang Q.-Q., Cui Y.-W., Zhang H.-H., Chang F., Zhu B.-H., Yu S.-Y. (2019) C-doped ZnO decorated with Au nanoparticles constructed from the metal–organic framework ZIF-8 for photodegradation of organic dyes. *RSC Advances* 9 (22): 12689–12695.

Dash S. (2010) Kinetic modeling on drug release from controlled drug delivery systems *Acta Pol Pharm*

Deac A., Qi Q., Indulkar A. S., Purohit H. S., Gao Y., Zhang G. G., Taylor L. S. (2022) Dissolution mechanisms of amorphous solid dispersions: role of drug load and molecular interactions. *Molecular Pharmaceutics* 20 (1): 722–737.

Dobson J. (2006) Magnetic nanoparticles for drug delivery. *Drug Development Research* 67 (1): 55–60.

Eiras D., Labreche Y., Pessan L. (2016) Ultem®/ZIF-8 Mixed Matrix Membranes for Gas Separation: Transport and Physical Properties. *Materials Research* 19

Elzoghby A. O., Helmy M. W., Samy W. M., Elgindy N. A. (2013) Micellar delivery of flutamide via milk protein nanovehicles enhances its antitumor efficacy in androgen-dependent prostate cancer rat model. *Pharm Res.* 30 (10): 2654–63.

Esmaeili J., Barati A., Salehi E., Ai J. (2023) Reliable Kinetics for Drug Delivery with a Microfluidic Device Integrated with the Dialysis Bag. *Molecular Pharmaceutics* 20 (2): 1129–1137.

Esmaeili J., Pirzadeh K., Pakrooyan M., Lukolayeh M. Esmaeilpour, Kırboğa K. K. (2024) Synthesis of cellulose nanocrystals from spinach waste for insulin delivery: comparison to chitosan nanoparticles. *New Journal of Chemistry* 48 (17): 7953–7963.

Faheem A. M., Abdelkader D. H. (2020) Novel drug delivery systems, Engineering drug delivery systems. Elsevier:1–16.

Freund R., Zaremba O., Arnauts G., Ameloot R., Skorupskii G., Dincă M., Bavykina A., Gascon J., Ejsmont A., Goscianska J. (2021) The current status of MOF and COF applications. *Angewandte Chemie International Edition* 60 (45): 23975–24001.

Gao J., Chu W., Ding X., Ding L., Guo Q., Fu Y. (2023) Degradation Kinetic Studies of BSA@ZIF-8 Nanoparticles with Various Zinc Precursors, Metal-to-Ligand Ratios, and pH Conditions. *ACS Omega* 8:44601–44610.

Hamishehkar H., Ghanbarzadeh S., Sepehran S., Javadzadeh Y., Adib Z. M., Kouhsoltani M. (2016) Histological assessment of follicular delivery of flutamide by solid lipid nanoparticles: potential tool for the treatment of androgenic alopecia. *Drug Dev Ind Pharm* 42 (6): 846–53.

He Q., Jiang Z., Jiang H., Han S., Yang G., Yuan X., Zhu H. (2024) Embedding AIE-type Ag 28 Au 1 nanoclusters within ZIF-8 for improved photodynamic wound healing through bacterial eradication. *Nanoscale* 16 (30): 14310–14318.

Hu Y., Kazemian H., Rohani S., Huang Y., Song Y. (2011) In situ high pressure study of ZIF-8 by FTIR spectroscopy. *Chemical Communications* 47 (47): 12694–12696.

Hu Y., Liu Z., Xu J., Huang Y., Song Y. (2013) Evidence of pressure enhanced CO_2 storage in ZIF-8 probed by FTIR spectroscopy. *Journal of the American Chemical Society* 135 (25): 9287–9290.

J. Yang P. Xiong Y. Li M. Wei C. Zheng (2014) Zn-doped Ni-MOF material with a high supercapacitive performance *Journal of Materials Chemistry A* 2 (44): 19005–19010.

Jiang H.-L., Liu B., Akita T., Harut M., et al. (2009) Au@ZIF-8: CO Oxidation over Gold Nanoparticles Deposited to Metal-Organic Framework. *Journal of the American Chemical Society* 131 (32): 11302–3.

Jiang X., Chen H.-Y., Liu L.-L., Qiu L.-G., Jiang X. (2015) Fe_3O_4 embedded ZIF-8 nanocrystals with ultra-high adsorption capacity towards hydroquinone. *Journal of Alloys and Compounds* 646:1075–1082.

Kang Y., Zhang L., Wang W., Yu F. (2021) Ethanol sensing properties and first principles study of Au supported on mesoporous ZnO derived from metal organic framework ZIF-8. *Sensors* 21 (13): 4352.

Khorshidian A., Sharifi N., Kheirabadi F. Choupani, Rezaei F., Sheikholeslami S. A., Ariyannejad A., Esmaeili J., Basati H., Barati A. (2024) In Vitro Release of Glycyrrhiza Glabra Extract by a Gel-Based Microneedle Patch for Psoriasis Treatment. *Gels*

Kida K., Okita M., Fujita K., S. Tanaka Y. (2013) Miyake, Formation of high crystalline ZIF-8 in an aqueous solution. *CrystEngComm* 15 (9): 1794–1801.

Koch D. C., Jang H. S., O'Donnell E. F., Punj S., Kopparapu P. R., Bisson W. H., Kerkvliet N. I., Kolluri S. K. (2015) Anti-androgen flutamide suppresses hepatocellular carcinoma cell proliferation via the aryl hydrocarbon receptor mediated induction of transforming growth factor-β1. *Oncogene* 34 (50): 6092–104.

Lei Z., Tang Q., Ju Y., Lin Y., Bai X., Luo H., Tong Z. (2020) Block copolymer@ ZIF-8 nanocomposites as a pH-responsive multi-steps release system for controlled drug delivery. *Journal of Biomaterials Science, Polymer Edition* 31 (6): 695–711.

Li S., Wang F., Xie Z., Ng D., Shen B. (2023) A novel core-shell structured Fe@ CeO_2-ZIF-8 catalyst for the reduction of NO by CO. *Journal of Catalysis* 421:240–251.

Liu A., Chen J., Li X., Cheng P., Wen L. (2007) Study of Drug Loading Distribution of Porous Hollow Nano-Carriers. *Journal of Chemical Engineering of Chinese Universities* 21 (5): 832.

Liu J., Wöll C. (2017) Surface-supported metal–organic framework thin films: fabrication methods, applications, and challenges. *Chemical Society Reviews* 46 (19): 5730–5770.

Lou Y., Song F., Cheng M., Hu Y., Chai Y., Hu Q., Wang Q., et al. (2023) Effects of the CYP3A inhibitors, voriconazole, itraconazole, and fluconazole on the pharmacokinetics of osimertinib in rats. *PeerJ* 11:e15844.

Lu S., Hummel M., Chen K., Zhou Y., Kang S., Gu Z. (2020) Synthesis of Au@ ZIF-8 nanocomposites for enhanced electrochemical detection of dopamine. Electrochemistry Communications:106715.

Mirsafaei R., Varshosaz J. (2020) Polyacrylamide-punicic acid conjugate-based micelles for flutamide delivery in PC3 cells of prostate cancer: synthesis, characterisation and cytotoxicity studies. *IET Nanobiotechnol* 14 (5): 417–422.

Palvai S., Kpeglo D., Newham G., Peyman S. A., Evans S. D., Ong Z. Y. (2024) Free-Standing Hierarchically Porous Silica Nanoparticle Superstructures: Bridging the Nano-to Microscale for Tailorable Delivery of Small and Large Therapeutics. *ACS Applied Materials & Interfaces* 16 (5): 5568–5581.

Panda M. K., Panda S. K., Singh Y. D., Jit B. P., Behara R. K., Dhal N. K. (2020) Role of nanoparticles and nanomaterials in drug delivery: an overview. *Advances in Pharmaceutical Biotechnology: Recent Progress and Future Applications.,* 247–265.

Pourmadadi M., Omrani Z., Forootan Z., Ebadi M. S., Yazdian F. (2023) UiO-66 nanoparticles as a drug delivery system: A comprehensive review. *Journal of Drug Delivery Science and Technology* 86:104690.

Proenza Y. G., Longo R. L. (2019) Simulation of the Adsorption and Release of Large Drugs by ZIF-8. *Journal of Chemical Information and Modeling* 60 (2): 644–652.

Quintero-Álvarez F. G., Rojas-Mayorga C. K., Mendoza-Castillo D. I., Aguayo-Villarreal I. A., Bonilla-Petriciolet A. (2022) Physicochemical modeling of the adsorption of pharmaceuticals on MIL-100-Fe and MIL-101-Fe MOFs. *Adsorption Science & Technology* 2022:4482263.

Reshimi S., Jihu K. R., Suma S., Anoop S. N. (2023) Folic acid grafted aminated zeoliticimidazoloate framework (ZIF-8) as pH responsive drug carrier for targeted delivery of curcumin. *J. Drug Deliv. Technol.* 79:104098.

Sabale V., Nikam M., Sabale P. (2024) Formulation, Optimization and *In Vitro* Studies of Flutamide-loaded Nanostructured Lipid Carrier Based Oral Drug Delivery for Enhanced Anticancer Activity. *Journal of Pharmaceutical Innovation* 19 (5): 53.

Sanvicens N., Marco M. P. (2008) Multifunctional nanoparticles–properties and prospects for their use in human medicine. *Trends in Biotechnology* 26 (8): 425–433.

Senjković R., Jalšenjak I. (1981) Surface topography of microcapsules and the drug release. *Journal of Pharmacy and Pharmacology* 33 (1): 665–666.

Talevi A., Ruiz M. E. (2022) Korsmeyer-peppas, peppas-sahlin, and brazel-peppas: models of drug release, The ADME encyclopedia: A comprehensive guide on biopharmacy and pharmacokinetics. Springer:613–621.

Teleanu D. M., Negut I., Grumezescu V., Grumezescu A. M., Teleanu R. I. (2019) Nanomaterials for drug delivery to the central nervous system. *Nanomaterials* 9 (3): 371.

Tongeren T. C. A. van, Carmichael P. L., Rietjens I., Li H. (2022) Next Generation Risk Assessment of the Anti-Androgen Flutamide Including the Contribution of Its Active Metabolite Hydroxyflutamide. *Front Toxicol* 4:881235.

Wang Q., Sun Y., Li S., Zhang P., Yao Q. (2020) Synthesis and modification of ZIF-8 and its application in drug delivery and tumor therapy. *RSC Advances* 10 (62): 37600–37620.

Wang X., Lu H., Liao B., Li G., Chen L. (2023) Facile synthesis of layered double hydroxide nanosheets assembled porous structures for efficient drug delivery. *RSC Advances* 13:12059–12064.

Wang Y., Zeng M., Fan T., Jia M., Yin R., Xue J., Xian L., Fan P., Zhan M. (2024) Biomimetic ZIF-8 nanoparticles: A novel approach for biomimetic drug delivery systems. *International Journal of Nanomedicine,* 5523–5544.

Xu Y., Wang S., Xiong J., Zheng P., Zhang H., Chen S., Ma Q., Shen J., Velkov T., Dai C. (2021) A Novel Fe_3O_4-Doped Metal-Organic Framework for Chemo/Chemodynamic Synergistic Therapy Via Triggering Ferroptosis. *Chemodynamic Synergistic Therapy Via Triggering Ferroptosis.*